Redox Biology 91 (2026) 104094

Contents lists available at ScienceDirect

Redox Biology

journal homepage: www.elsevier.com/locate/redox

Bidirectional coupling of neuronal Ca^{2+} and nitric oxide signals visualized by a dual biosensor

Asel Aydeger [a,b], Sena Yildirim [a,b], Tuba Akgul Caglar [a], Asal Ghaffari Zaki [a,b], Seyed Mohammad Miri [a,b], Joudi Armouch [a,c], Hamzah Issa [a,b], Esranur Yavuz [a,b], Arda Kebapçı [a], Mehmet Koçak [d,e,f], Roland Malli [g], Pierre Gressens [h], Nikolaus Plesnila [i,j], Emrah Eroglu [a,k,*]

[a] Research Institute for Health Sciences and Technologies (SABITA), Istanbul Medipol University, Istanbul, 34810, Türkiye
[b] Graduate School of Health Sciences, Istanbul Medipol University, Istanbul, 34810, Türkiye
[c] Biomedical Engineering and Bioinformatics, Graduate School of Engineering and Natural Sciences, Istanbul Medipol University, Istanbul, 34810, Türkiye
[d] International School of Medicine, Istanbul Medipol University, Istanbul, 34810, Türkiye
[e] Department of Biostatistics and Medical Informatics, Istanbul Medipol University, Istanbul, 34810, Türkiye
[f] Multi-Omics Design and Analysis Studio (MODAS-SABITA), Istanbul Medipol University, Istanbul, 34810, Türkiye
[g] Core Facility Bioimaging, Centre for Medical Research, Medical University of Graz, Graz, 8010, Austria
[h] Université Paris Cité, Inserm, NeuroDiderot, Paris, 75019, France
[i] Institute for Stroke and Dementia Research (ISD), LMU University Hospital, LMU Munich, Munich, 81377, Germany
[j] Munich Cluster of Systems Neurology (SyNergy), Munich, 81377, Germany
[k] Molecular Biology, Genetics, and Bioengineering Program, Sabanci University, Istanbul, 34956, Türkiye

ARTICLE INFO

Keywords:
Ca^{2+} signaling
Nitric oxide
Neuronal nitric oxide synthase (nNOS)
Hippocampal neurons
Dual biosensor

ABSTRACT

Nitric oxide (NO) and calcium (Ca^{2+}) are tightly interconnected mediators of neuronal signaling, yet their dynamic relationship in primary neurons has remained widely unexplored. Here we report a bicistronic dual biosensor that combines jGCaMP8s for high-sensitivity Ca^{2+} imaging with the orange fluorescent NO reporter O-geNOps, delivered by adeno-associated virus (AAV) to primary hippocampal neurons. We establish imaging conditions optimized for physiological temperature and oxygen, which critically shape NO bioavailability. Under these conditions, spontaneous Ca^{2+} spikes and network activity are largely insufficient to elicit detectable NO production, whereas robust Ca^{2+} elevation by high extracellular K^+ (50 mM) or glutamate (30 μM) evokes robust NO signals that surpass responses to exogenous NO donors. Conversely, both endogenous and exogenously applied NO dampen spontaneous Ca^{2+} spikes, revealing feedback control of neuronal excitability in the hippocampus. Together, these findings demonstrate bidirectional functional coupling between Ca^{2+} and NO signals in primary hippocampal neurons and introduce an informative approach for dual-color visualization of both messengers under near-physiological conditions.

1. Introduction

Ca^{2+} ions and NO are second messengers in neurons, coordinating processes from synaptic transmission to transcriptional regulation [1–3]. Ca^{2+} acts as a universal signaling ion that shapes neuronal excitability, action potential firing, neurotransmitter release, and activity-dependent gene expression [4]. NO, which is produced mainly by neuronal nitric oxide synthase (nNOS) in neurons, is a gaseous signaling mediator with unique biophysical properties that enable rapid membrane diffusion and modulation of both intra- and intercellular communication [5]. In addition, NO is a key regulator of redox-dependent processes in the nervous system, influencing mitochondrial respiration, metabolic coupling, vascular tone, and redox-sensitive protein modifications [6–10]. Both the enzymatic production of NO and its lifetime are strongly influenced by oxygen tension and temperature, making these basic physical parameters critical for

This article is part of a special issue entitled: The role of NO in redox signaling and disease published in Redox Biology.

* Corresponding author. Research Institute for Health Sciences and Technologies (SABITA), Istanbul Medipol University, Istanbul, 34810, Türkiye.
E-mail address: emrah.eroglu@medipol.edu.tr (E. Eroglu).

https://doi.org/10.1016/j.redox.2026.104094
Received 4 December 2025; Received in revised form 16 January 2026; Accepted 16 February 2026
Available online 17 February 2026

interpreting NO-dependent signaling [11].

Ca^{2+} and NO are tightly interconnected in neurons, forming a dynamic bidirectional signaling [12]. Ca^{2+} directly controls NO production by activating nNOS through Ca^{2+}/calmodulin binding [13]. Conversely, NO shapes Ca^{2+} homeostasis by acting on voltage-gated Ca^{2+} channels, NMDA receptors, ryanodine receptors, and mitochondrial Ca^{2+} handling mechanisms [14,15]. Through S-nitrosylation and cGMP–PKG signaling, NO can modulate ion channel conductance, synaptic strength, and metabolic activity [16,17]. Together, these reciprocal interactions couple neuronal excitability to metabolic and redox demands, helping to prevent excessive Ca^{2+} influx and limiting oxidative or nitrosative stress [18–20]. Thus, the Ca^{2+}–NO interplay is a central hub that coordinates electrical activity with redox balance and energy demand in neurons [9].

Although the Ca^{2+}–NO axis helps maintain neuronal balance, it is easily disrupted [21]. In ischemia [22], traumatic brain injury [23], and Alzheimer's [24] and Parkinson's [25], high Ca^{2+} can over activate nNOS, leading to excess NO and peroxynitrite [26]. This causes

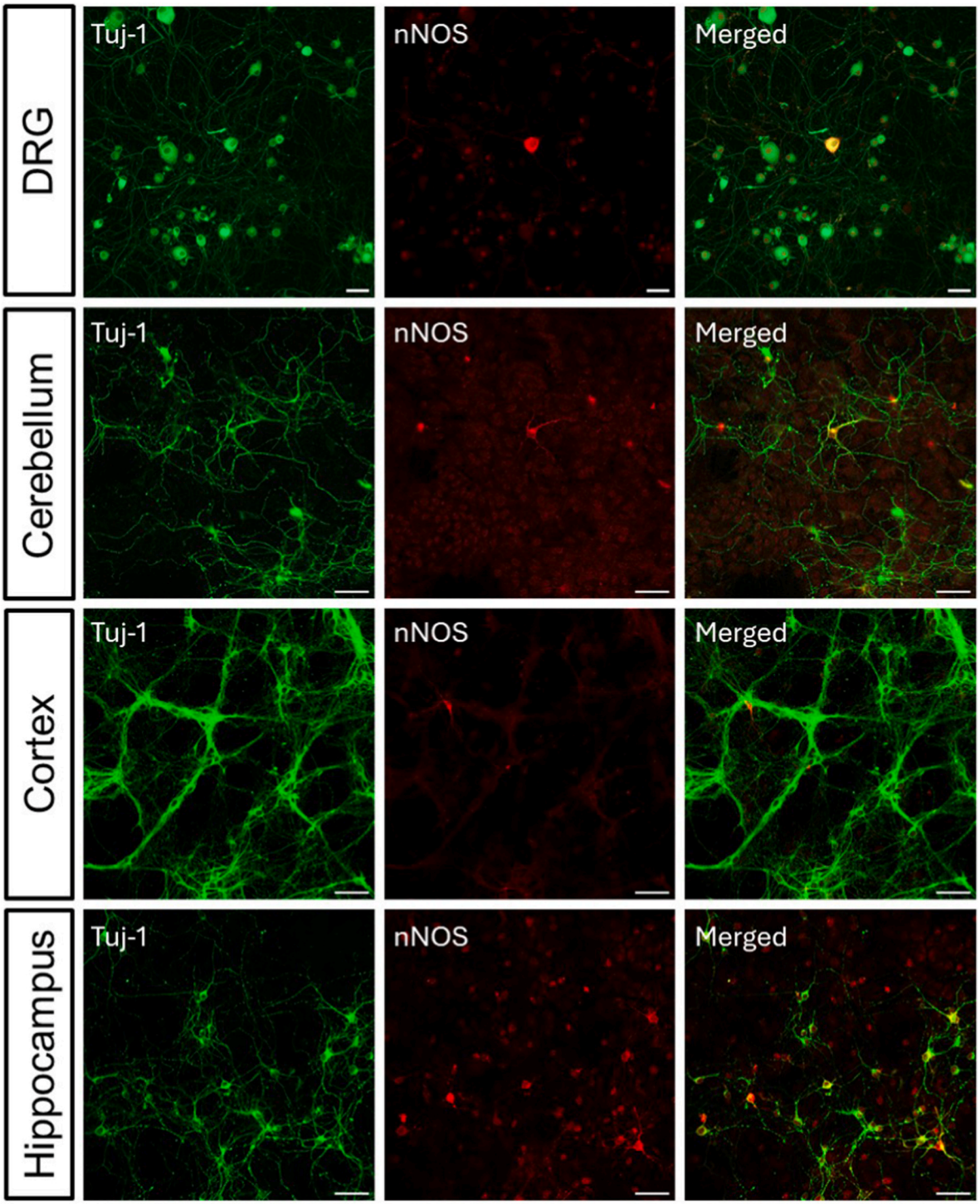

Fig. 1. Differential nNOS expression across nervous system tissues. High-resolution confocal micrographs of co-cultures from dorsal root ganglion (DRG), cerebellum, cortex, and hippocampus. Except for DRG, tissues were isolated from neonatal mice. Cultures were immunolabeled for Tuj1 (neuronal βIII-tubulin; left) and nNOS (middle). Representative images from four independent experiments (n = 4). Scale bar, 50 μm.

mitochondrial dysfunction, protein nitration, lipid peroxidation, and loss of synaptic integrity [27,28]. The reverse is also true: weak or faulty NO signaling can disturb Ca^{2+} buffering, impair synaptic plasticity, and reduce local blood flow, increasing neuronal vulnerability [29–32]. Many of these conditions are also associated with changes in pericellular oxygen, making it important to study Ca^{2+} and NO under physiological oxygen levels (~1–5 kPa O_2) [33–35], rather than the atmospheric oxygen (~18–21 kPa O_2) that is still used in most in vitro studies [36,37]. Therefore, tracking Ca^{2+} and NO in real time under defined oxygen and temperature conditions is key to understanding how redox signaling links neuronal activity, energy use, and oxidative stress responses [38].

Monitoring Ca^{2+} and NO together in neurons with adequate temporal and spatial resolution is still difficult [39]. Many synthetic NO probes respond slow and irreversible, have limited specificity, high background, or photobleaching [40,41]. Genetically encoded Ca^{2+} indicators, including jGCaMP variants, are well established and widely used for Ca^{2+} imaging in neurons [42]. In primary neurons, pairing these indicators with NO sensors mainly raises practical considerations such as co-expression efficiency, spectral separation, and cellular load. Genetically encoded NO reporters such as O-geNOps have improved NO imaging [43,44], yet concurrent Ca^{2+}–NO measurements in primary neurons remain limited, especially under controlled oxygen and temperature [45].

To address these challenges, we engineered an AAV-delivered bicistronic dual reporter that co-expresses the orange NO biosensor O-geNOps [36] and the high-sensitivity Ca^{2+} indicator jGCaMP8s [42] in primary hippocampal neurons. The design supports balanced expression and is compatible with redox- and activity-sensitive neuronal environments. Using this imaging system, we tracked Ca^{2+} and NO on the level of individual cells in real time and tested how temperature, oxygen, and iron availability affect NO bioavailability under near-physiological conditions. This platform thus enables simultaneous Ca^{2+}–NO imaging in single cells under defined, near-physiological conditions and provides a practical basis to dissect oxygen-dependent redox mechanisms that regulate neuronal excitability and metabolism in the hippocampus.

2. Results

To identify a primary neuronal preparation with robust neuronal nitric oxide synthase (nNOS) expression for Ca^{2+} and NO imaging, we first compared different regions of the murine nervous system. Co-cultures derived from adult dorsal root ganglia (DRG) and from neonatal cortex, cerebellum, and hippocampus were stained for the neuronal marker Tuj1 (βIII-tubulin) and nNOS (Fig. 1). In DRG (17%, ±SD 15,5), cortex (29% ± SD 5.1), and cerebellar cultures (24% ± SD 16.3), nNOS immunoreactivity was detected only in a limited subset of Tuj1-positive neurons, often with relatively weak somatic and neuritic labeling. In contrast, hippocampal cultures displayed a high density of Tuj1-positive neurons with strong nNOS staining in cell bodies and processes, indicating that nNOS-positive neurons are particularly abundant in this preparation (Fig. 1, lower images) (33%, ±SD 4.9). Based on this expression pattern, primary hippocampal neurons were selected as the model system for subsequent functional Ca^{2+} and NO imaging experiments.

To enable simultaneous monitoring of Ca^{2+} and NO, we initially co-transduced primary hippocampal neurons with two separate AAV2 vectors encoding cytosolic O-geNOps-NES and GCaMP6s under the hSyn promoter (Supplementary Fig. S1). Although both probes were functional, wide-field imaging revealed highly heterogeneous expression levels, with many neurons displaying strong fluorescence from only one of the reporters. In cells with prominent O-geNOps expression, depolarization with 50 mM K^+ reliably elicited robust NO signals, whereas the corresponding GCaMP6s responses were small or undetectable (Supplementary Fig. S1). Conversely, neurons with higher GCaMP6s expression typically exhibited weak O-geNOps signals (data not shown). Thus, equimolar co-expression of the two biosensors in the same neuron could not be achieved in a consistent and experimentally useful manner using separate AAV2 vectors, motivating the development of a bicistronic dual-reporter design.

To optimize Ca^{2+} reporting for dual-imaging with NO, we next compared two members of the latest jGCaMP8 family in a defined cellular system. HEK293T cells expressing either jGCaMP8s or jGCaMP8f were stimulated with various ATP concentrations, and population responses were recorded over time (Supplementary Fig. S2 A,B). Both sensors reported ATP-evoked Ca^{2+} elevations, but jGCaMP8s consistently produced larger fluorescence changes, particularly at low agonist concentration. At 5 μM ATP, peak ΔF was significantly higher for jGCaMP8s than for jGCaMP8f (Fig. S2C). In addition, jGCaMP8s signals displayed a broader full width at half maximum (FWHM), indicating more sustained responses (Fig. S2D), and a lower desensitization index during repeated stimulation (Fig. S2E). These data demonstrate that jGCaMP8s provides higher sensitivity and stability for detecting small and prolonged Ca^{2+} transients, and therefore we selected jGCaMP8s as the Ca^{2+} reporter for our bicistronic Ca^{2+}/NO biosensor construct.

To achieve stoichiometric co-expression of the Ca^{2+} and NO reporters, we engineered a bicistronic construct in which cytosolic O-geNOps and jGCaMP8s are separated by a self-cleaving P2A peptide and flanked by nuclear export signals (NES), under control of the human synapsin (hSyn) promoter (Fig. 2A). For initial characterization prior to moving to complex primary neuronal cultures, we first tested the dual biosensor via transient transfection in HEK293T cells. This resulted in robust and homogeneous fluorescence of both probes in the same cells (Supplementary Fig. S3). Sequential stimulation with ATP and an NO donor confirmed that the two channels were functional and spectrally separable (Supplementary Fig. S3D and E): ATP elicited repetitive Ca^{2+} transients reported by jGCaMP8s with no detectable O-geNOps response, due to the lack of any NOS expression in HEK293T cells [39], whereas subsequent application of the NO donor produced a sustained O-geNOps signal without affecting jGCaMP8s fluorescence (Supplementary Fig. S3 B).

We next packaged the bicistronic cassette into an adeno-associated virus and transduced primary hippocampal neurons. Confocal imaging showed co-localized expression of O-geNOps and jGCaMP8s throughout the soma and neurites of individual neurons (Fig. 2B). Upon depolarization with high extracellular K^+ (50 mM), neurons displayed a rapid jGCaMP8s fluorescence increase followed by a slightly slower, longer-lasting rise in O-geNOps signal (Fig. 2C), demonstrating that the dual biosensor reports both cytosolic Ca^{2+} elevations and endogenous Ca^{2+}-triggered NO biosynthesis in the same primary hippocampal neuron under stimulation conditions relevant for subsequent experiments.

To approximate *in vivo*-like recording conditions for dual Ca^{2+}/NO imaging, we next examined how oxygen tension and temperature affect probe performance in primary hippocampal neurons. Under conventional conditions (room air, room temperature), depolarization with 50 mM K^+ evoked a relatively small O-geNOps response, whereas subsequent application of the NO donor produced only modest increases in O-geNOps fluorescence (Fig. 3A, left). When neurons were adapted to physioxia (5 kPa O_2) directly after isolation for ≥5 days and imaged at room temperature, K^+-evoked NO signals were significantly larger, while Ca^{2+} transients remained unchanged (Fig. 3A, middle; Fig. 3B). Raising the temperature to 37 °C under the same 5 kPa O_2 conditions further enhanced the K^+-induced NO response without altering the magnitude of jGCaMP8s signals (Fig. 3A, right; Fig. 3B). In contrast, O-geNOps responses to exogenous NO donor were comparable across all three conditions (Fig. 3B, middle), indicating that physioxia and physiological temperature primarily increase activity-dependent NO production rather than sensor responsiveness. While the on-kinetics of the high K^+-evoked NO increase were comparable across all three conditions, only physiological oxygen and temperature promoted more rapid NO decay in cells (Supplementary Fig. S5).

Because geNOps function depends on non-heme ferrous iron availability [43], we also optimized iron supplementation in neurons adapted

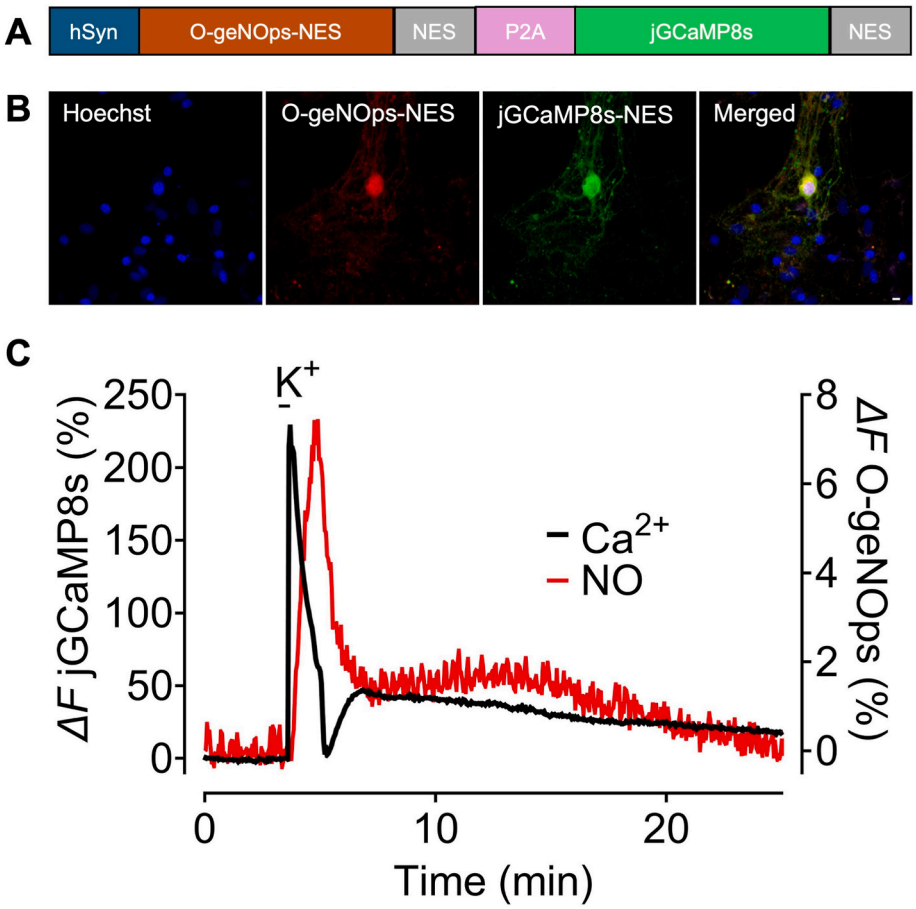

Fig. 2. Dual imaging of nitric oxide and Ca^{2+} in hippocampal neurons. (A) Schematic of the bicistronic construct encoding O-geNOps-NES and jGCaMP8s-NES under the human synapsin promoter (hSyn), separated by a P2A peptide **(B)** High-resolution confocal images of hippocampal neurons expressing the bicistronic NO–Ca^{2+} reporter. From left to right: Hoechst nuclear stain, O-geNOps-NES, cytosolic jGCaMP8s-NES, and the merged channels. Hoechst-stained nuclei include neighboring astrocytes and non-neuronal cells, whereas NO and Ca^{2+} signals originate solely from transduced neurons. Scale bar, 10 μm. Images acquired with a 20 × objective. **(C)** Real-time traces from multispectral imaging showing O-geNOps (NO) and jGCaMP8s (Ca^{2+}), color-coded as indicated, in response to KCl (50 mM); stimulus timing is indicated by the bars. Data are representative of 15 cells recorded across ≥5 independent experiments (n = 15 (cells); ≥5 experiments).

to 5 kPa O_2. Notably, O-geNOps reported clear NO donor responses even without exogenous iron (Supplementary Fig. S6), in contrast to earlier observations in non-neuronal cells. Short pretreatment with 150 μM $FeSO_4$ and 300 μM vitamin C significantly augmented NO-evoked O-geNOps signals, whereas higher concentrations (300/500 μM) did not provide additional benefit (Supplementary Fig. S6 A,B). We therefore used 150 μM $FeSO_4$ plus 300 μM vitamin C for 15 min as a standard loading protocol at physiological temperature and 5 kPa pericellular oxygen in all subsequent experiments.

We next used the dual biosensor to relate endogenous NO production to different modes of Ca^{2+} activity in primary hippocampal neurons. Under physioxic, 37 °C conditions, application of the NO donor PROLI NONOate (20 μM) produced a robust O-geNOps signal without evoking additional Ca^{2+} transients (Fig. 4A). Notably, both exogenous NO and endogenously generated NO were consistently associated with a marked suppression of spontaneous Ca^{2+} spiking, which reappeared once the NO signal decayed (Fig. 4A–C). Statistical quantification showed that during exogenous NO administration and NO endogenous generation, spontaneous Ca^{2+} spike frequency and amplitudes significantly decreased (Supplementary Fig. S8).

To probe the Ca^{2+} dependence of nNOS activation, we compared different depolarization strengths using increasing K^+ concentrations. While 50 mM K^+ reliably elicited large and prolonged NO responses that exceeded those obtained with the NO donor (Fig. 4A), lower K^+ concentrations (10–30 mM) triggered pronounced Ca^{2+} oscillations but only weak O-geNOps signals (Fig. 4D). Even when 10 mM K^+ induced long-lasting, high-frequency Ca^{2+} oscillations, the corresponding NO response remained small (Fig. 4E). Importantly, following the first Ca^{2+} peak upon KCl administration, a delayed and more sustained rise in NO was observed. Quantitative analysis showed that geNOps signals peaked shortly after stimulation (74,85, ±SD 17,22 s) (Supplementary Fig. S7). These observations indicate that, under physiological recording conditions, spontaneous and modest depolarization-evoked Ca^{2+} activity is insufficient to robustly activate nNOS, whereas strong depolarization with 50 mM K^+ is required to generate substantial endogenous NO production.

3. Discussion

In this study we set out to directly visualize the interplay between Ca^{2+} and nitric oxide signaling in primary hippocampal neurons, a relationship that has so far been inferred mainly from indirect measurements [30,46–48]. To this end, we (I) developed a bicistronic AAV-based dual biosensor combining the high-sensitivity Ca^{2+} indicator jGCaMP8s [42] with the NO reporter O-geNOps [43] and (II) optimized its use under physioxic, near-physiological recording conditions. Using this tool, we show (III) that only strong depolarization elicits robust endogenous NO production, (IV) whereas spontaneous or modest Ca^{2+} activity is largely insufficient to activate nNOS. We further demonstrate (V) that both exogenous and endogenous NO transiently suppress spontaneous Ca^{2+} spiking, revealing a bidirectional coupling between these two signaling pathways in intact primary hippocampal neurons.

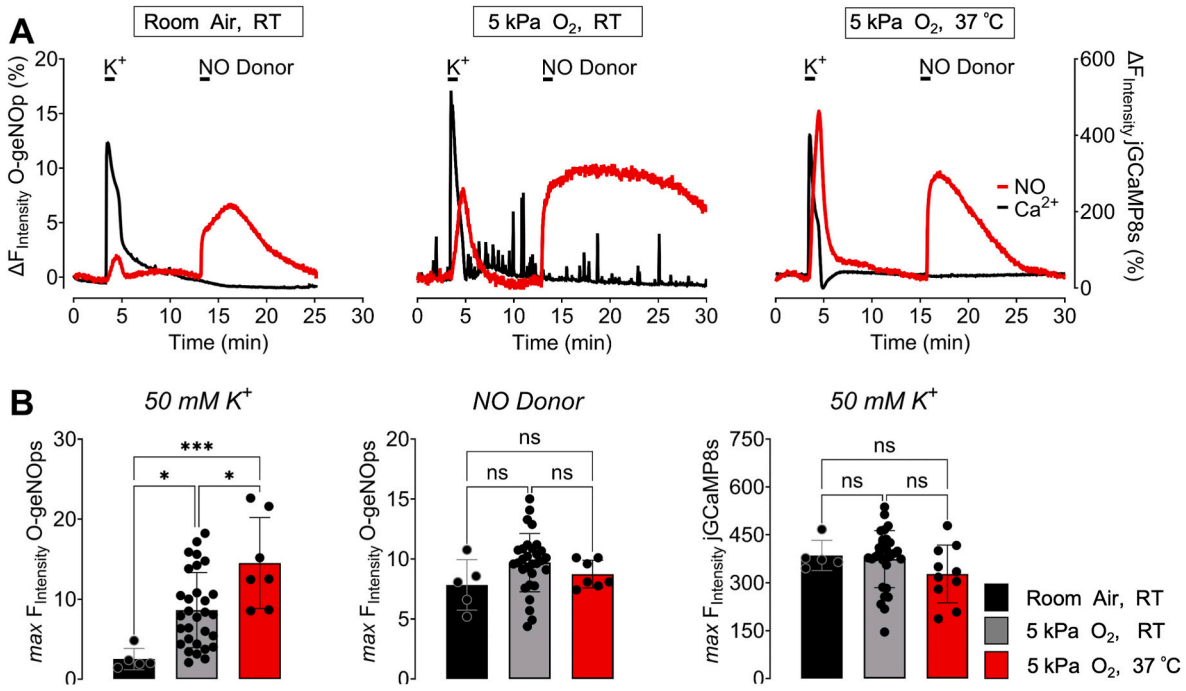

Fig. 3. Imaging nitric oxide and Ca^{2+} signals under physiological conditions. (A) Representative real-time traces from hippocampal neurons expressing the bicistronic construct during stimulation with high K^+ (50 mM) and PROLI NONOate (20 μM) under three conditions: room temperature (RT) in room air (~21 kPa O_2; left, n = 3/5), RT after adaptation to 5 kPa O_2 (≥5 days; middle, n = 3/30), and 37 °C after adaptation to 5 kPa O_2 (right, n = 3/7). **(B)** Quantification of peak O-geNOps responses to 50 mM K^+ (left) and to 20 μM PROLI NONOate (middle), and peak jGCaMP8s responses to 50 mM K^+ (right) across the three conditions: RT/room air (black), RT/5 kPa O_2-adapted (grey), and 37 °C/5 kPa O_2-adapted (red). Data are mean ± SD; n (cells) per condition: 5–30. Statistics: ordinary one-way ANOVA with Tukey's multiple-comparisons test. $P < 0.05$; $^{**}p < 0.001$.

Our initial analysis of nNOS distribution confirmed that NO signaling is particularly prominent in the hippocampus. Among the neuronal cultures tested—cortex, cerebellum, DRG, and hippocampus—hippocampal neurons displayed the most abundant and intense nNOS immunoreactivity in Tuj1-positive cells (Fig. 1). Beyond the higher nNOS abundance, we selected the hippocampus also for practical and methodological reasons. The hippocampus is a well-defined and anatomically restricted structure, which facilitates reproducible microdissection and minimizes the risk of contaminating the preparation with adjacent brain regions. This is particularly important for sample standardization across experiments, as cortical dissections are more extensive and can carry a higher risk of inadvertent inclusion of neighboring areas. Thus, hippocampal cultures provide both a robust nNOS-positive neuronal population and a more standardized, contamination-resistant starting material for consistent Ca^{2+}–NO imaging. This is consistent with previous reports that nNOS is widely expressed in the CNS but especially enriched in hippocampal CA1 interneurons and pyramidal neurons [49], where NO acts as a retrograde messenger involved in long-term potentiation [49,50], synaptic plasticity, and regulation of local microcirculation [51,52]. The strong nNOS expression signal we observed therefore aligns well with the established role of NO in hippocampal information processing and neurovascular coupling [53–55].

On this basis, we selected primary hippocampal neurons as our model system, not to comprehensively map regional differences in NO signaling, but to ensure robust endogenous NO generation in a physiologically relevant, highly active neuronal population. Our goal was to measure NO and Ca^{2+} simultaneously with sufficient signal-to-noise to dissect their dynamic relationship, rather than to compare absolute nNOS levels across brain regions. We acknowledge that distinct neuronal subtypes and brain areas differ in nNOS expression and NO signaling [56], and that the quantitative features of Ca^{2+}–NO coupling may vary accordingly. However, the hippocampal preparation provides a stringent testbed in which high nNOS abundance and well-characterized NO-dependent plasticity create favorable conditions for resolving the bidirectional interaction between Ca^{2+} and NO with our dual biosensor approach.

Our initial co-transduction experiments with two independent AAV2 vectors encoding O-geNOps and GCaMP6s revealed a practical limitation of dual-vector strategies: despite using the same neuronal promoter and comparable viral doses, equimolar expression of both probes in the same neuron was rarely achieved (Supplementary Fig. S1). This likely reflects stochastic differences in viral uptake, genome copy number, and promoter activity at the single-cell level, which become particularly evident in primary neurons with limited transduction efficiency [57]. In many cells one reporter dominated while the other was barely detectable, making quantitative, cell-resolved Ca^{2+}/NO comparisons unreliable. Bicistronic expression cassettes have emerged as a powerful way to enforce stoichiometric co-expression [58], and we adopted this strategy here. By linking O-geNOps and GCaMP8s via a P2A peptide under the hSyn promoter, we were able to drive robust, near-equimolar expression of both reporters from a single AAV genome, despite the restricted packaging capacity of AAV. The resulting construct remained within size limits and nevertheless produced bright, well-distributed fluorescence in both HEK293T cells and primary hippocampal neurons (Fig. 2 and Supplementary Fig. 3).

An additional, more practical design consideration emerged from our bicistronic constructs. In line with anecdotal reports from other multicistronic systems, we found that the reporter placed in the first position upstream of the P2A sequence was consistently expressed more strongly than the downstream reporter. In our hands, red-shifted FP–based probes showed clearly better expression when positioned before, rather than after, the GFP-based construct. Although these observations are not systematically quantified and therefore not shown, they guided our final design, in which O-geNOps was deliberately placed in the first position and GCaMP8s downstream of the P2A. This arrangement ensured robust NO reporter expression without compromising Ca^{2+} sensor performance and may be useful to consider for future dual- or multicistronic AAV

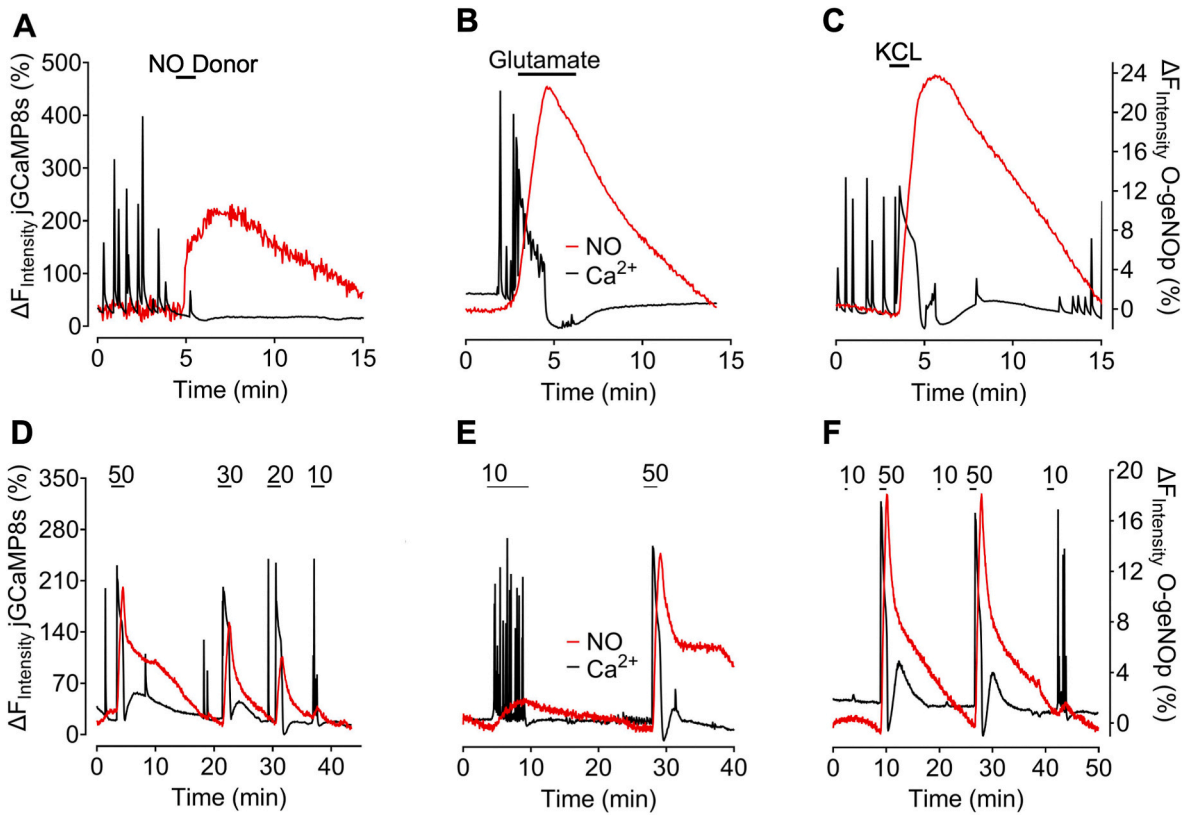

Fig. 4. Simultaneous Ca^{2+}Duplicate references have been removed and subsequent references renumbered.**and nitric oxide imaging in primary hippocampal neurons.** (A–C) Simultaneous Ca^{2+} (jGCaMP8s, black) and NO (O-geNOps, red) signals in response to **(A)** the NO donor PROLI NONOate (20 μM; applied at 4.5 min for 1 min) (n = 5/4) **(B)** glutamate (30 μM; applied at 3 min for 3 min) (n = 3/3), and **(C)** KCl (50 mM; applied at 3 min for 1 min) (n = 3/5). **(D–F)** Representative dual-channel recordings during stimulation with different KCl concentrations as indicated above the traces (10–50 mM; applied at 3 min for 1 min), illustrating the graded recruitment of NO production relative to depolarization-induced Ca^{2+} elevations.

designs where one probe is intrinsically dimmer or more demanding in terms of expression level which is particularly critical for in vivo experiments.

In parallel, we compared different GCaMP8 variants to identify an optimal Ca^{2+} reporter for probing nNOS activation thresholds (Supplementary Fig. S2). Although jGCaMP8f offers faster kinetics [42], its lower affinity for Ca^{2+} and higher desensitization index rendered it suboptimal for our purposes: repetitive Ca^{2+} spikes led to progressive signal attenuation, and small or brief Ca^{2+} elevations were reported with reduced sensitivity. In contrast, GCaMP8s displayed higher responsiveness to low micromolar ATP in HEK cells, broader signal integration, and greater stability during repeated stimulation, making it better suited to detect subtle Ca^{2+} changes that may or may not be sufficient to activate nNOS (Supplementary Fig. S2). Using this sensitive Ca^{2+} probe together with O-geNOps, we observed that strong depolarization evokes NO signals that surpass those produced by saturating NO donors, suggesting a remarkably high catalytic capacity and rapid activation of nNOS in hippocampal neurons (Figs. 3 and 4). While a direct comparison with endothelial NOS was beyond the scope of this work, our findings are in line with previous observations that neuronal NOS can generate NO on much faster timescales [39], underscoring the need for high-performance dual reporters to faithfully capture Ca^{2+}–NO coupling in these cells.

Our findings with the dual biosensor also underscore how strongly NO signaling in neurons depends on the ambient oxygen environment (Fig. 3). We and others have previously shown in non-neuronal systems that pericellular oxygen tension critically shapes NO bioavailability [36], with conventional room air culture conditions profoundly altering the proteome [35], Nrf2 activity [34], iron handling [36], and NO signaling [33,59]. Yet neurons are still routinely cultured and imaged at atmospheric oxygen. By adapting primary hippocampal neurons to physioxia [37] (5 kPa O_2) and imaging at 37 °C, we now demonstrate that endogenous, activity-dependent NO production is markedly enhanced under near-physiological conditions, whereas Ca^{2+} transients remain essentially unchanged (Fig. 3). This indicates that earlier work carried out at room air likely underestimated both the magnitude and the kinetics of neuronal NO signals and highlights the importance of controlling oxygen tension when investigating redox signaling in the nervous system.

A second, mechanistically relevant aspect of Fig. 3 and Supplementary Fig. S4 concerns the iron dependence of geNOps. In secondary cell lines such as HEK293 and HeLa cells, O-geNOps is essentially non-responsive in the absence of exogenous iron/vitamin C supplementation [36,39,43], reflecting limited ferrous iron availability. In contrast, primary hippocampal neurons adapted to physioxia showed clear O-geNOps responses to NO donors even without added iron, and only moderate iron/vitamin C pretreatment was sufficient to maximize signal amplitude (Supplementary Fig. S6). This suggests that freshly isolated, physiologically cultured neurons maintain a more favorable iron homeostasis for NO sensing than immortalized lines. Importantly, it also supports the feasibility of applying geNOps-based NO imaging in vivo, where systemic iron manipulation is difficult or undesirable. Importantly, this finding should be interpreted in the context of sensor performance rather than physiological regulation of neuronal iron homeostasis, and primarily serves to inform experimental design and optimization of geNOps-based NO imaging. Future in vivo studies in rodents or genetically tractable organisms such as Drosophila will be needed to define how tissue-specific iron handling and oxygen gradients jointly tune geNOps performance and, more broadly, neuronal NO signaling under truly native conditions.

Our final set of experiments refines how nNOS "reads" neuronal Ca^{2+} signals and feeds back onto excitability. Using the dual biosensor under physioxic, 37 °C conditions, we consistently found that neither spontaneous Ca^{2+} spikes nor prolonged oscillatory Ca^{2+} activity induced by mild depolarization (10 mM K^+) were sufficient to elicit robust NO production, even when Ca^{2+} oscillations were frequent and long-lasting (Fig. 4). By contrast, brief but strong depolarization with 50 mM K^+ reliably produced large O-geNOps responses that exceeded those elicited by exogenous NO donors (Fig. 4), indicating that only high-intensity Ca^{2+} signals cross the threshold needed for full nNOS activation in hippocampal neurons.

This threshold-like behavior is in line with the biophysics of Ca^{2+}/calmodulin (CaM)–dependent nNOS activation [60,61]. CaM binds Ca^{2+} with Kd values in the low micromolar range (~5×10^{-7} to 5×10^{-6} M), with the C-terminal EF hands showing particularly high affinity [62,63]. Constitutive NOS isoforms, including nNOS, require Ca^{2+}–CaM binding for catalytic activity, so effective activation is expected only when local Ca^{2+} rises into the upper nanomolar–micromolar range near open channels [64,65]. Our data support this view: "small" or moderate Ca^{2+} signals—whether spontaneous or driven by 10–30 mM K^+—clearly occur but do not translate into strong NO output, whereas intense depolarization with 50 mM K^+ crosses the Ca^{2+}/CaM threshold and yields a massive NO response. In other words, not every Ca^{2+} signal counts for NO production, consistent with the idea that nNOS functions as a high-threshold decoder of strong, high-frequency neuronal activity rather than a linear reporter of all Ca^{2+} fluctuations. It should also be noted that co-expression of a calmodulin-dependent Ca^{2+} biosensor could, in principle, compete with nNOS for Ca^{2+}/CaM binding and thereby alter the threshold for NO production. Additional experiments are required to determine how GCaMPs, compared with troponin C–based and other Ca^{2+} biosensors, affect endogenous Ca^{2+}-triggered neuronal NO synthesis [66].

An additional consideration concerns the stimulus-dependent mechanisms that engage nNOS, which differ substantially between glutamatergic activation and K^+-induced depolarization. Glutamate activates nNOS predominantly through NMDA receptor–mediated Ca^{2+} entry that is spatially organized by PSD95 scaffolding at postsynaptic sites, leading to a highly compartmentalized Ca^{2+}–nNOS coupling pathway [67]. Consistent with this architecture, our glutamate experiments showed an initial phase of recurrent Ca^{2+} spikes that did not immediately trigger NO production, followed only later by a larger, prolonged Ca^{2+} elevation that coincided with the onset of the NO signal (Fig. 4B). In contrast, high extracellular K^+ depolarizes the entire neuronal membrane and drives a rapid, spatially widespread Ca^{2+} influx through voltage-gated Ca^{2+} channels, which was followed almost immediately by a steep rise in NO (Fig. 4A, right panel). These distinct temporal patterns suggest that nNOS activation requires not only elevated Ca^{2+} but also specific spatial and amplitude thresholds that are reached more rapidly during strong, global depolarization than during synaptic receptor–mediated Ca^{2+} oscillations.

In addition, our recordings reveal clear feedback from NO onto Ca^{2+} dynamics which is in line with our previous observations in cardiac cells demonstrating the suppression of Ca^{2+} spiking in response to exogenous NO administration [43]. Both exogenous and endogenously produced NO transiently suppressed spontaneous Ca^{2+} spike-frequency and amplitude significantly, with activity resuming as NO levels declined (Fig. 4 and Supplementary Fig. S8). This is compatible with previous work showing that NO modulates neuronal excitability via multiple targets, including Ca^{2+}-activated K^+ channels and voltage-gated Ca^{2+} channels, leading in many contexts to a net reduction of Ca^{2+} entry and firing probability [20,48]. Although NO can also enhance specific Ca^{2+} channel subtypes in defined circuits [68], our observations in hippocampal neurons fit a predominantly negative-feedback role, where NO dampens ongoing activity once nNOS has been strongly engaged [69,70].

In the current study, we did not directly test NOS-dependence using pharmacological inhibitors. Although this approach is commonly used to probe enzymatic NO production, it is not readily interpretable in our neuronal culture system because the most potent NOS inhibitors are arginine-derived. Both our ongoing observations and published work indicate that arginine derivatives (and several other amino acids) can themselves suppress spontaneous Ca^{2+} spiking activity independently of NOS inhibition [21]. Thus, applying these inhibitors would introduce a strong confounding effect on the very Ca^{2+} activity readout used to infer endogenous NO signaling, preventing an unambiguous attribution of the observed responses to NOS blockade.

Taken together, these experiments demonstrate a truly bidirectional relationship:Ca^{2+} controls when and how much NO is produced, and NO in turn feeds back to sculpt the Ca^{2+} activity landscape. Crucially, this behavior could be resolved with high temporal precision only because our dual-biosensor approach allowed simultaneous, single-cell imaging of both signals under near-physiological conditions. Notably, in the original geNOp validation study, the differently colored geNOps showed responses to NO in the low-nanomolar range ($EC_{50} \approx$ O-geNOp 51.3 nM), demonstrating that the sensor can report low-nM NO signals. However, the NO sensitivity of our bicistronic dual-sensor configuration in hippocampal neurons has not been directly calibrated against defined nanomolar NO standards and may differ due to cellular context. Therefore, the absence of detectable NO signals under mild stimulation in Fig. 4 may reflect a detection-threshold limitation rather than a true lack of endogenous NO production. We accordingly temper our interpretation and state that strong depolarization robustly produces NO signals within the detectable range of the reporter, while subtler physiological NO elevations may require calibration and/or more sensitive detection approaches. A key open question that emerges from our work is not only when and how strongly nNOS is activated, but where within the neuron this Ca^{2+}–NO coupling is initiated and decoded. In the present study, both reporters were targeted to the cytosol via NES motifs, allowing us to capture integrated whole-cell Ca^{2+} and NO signals but not to resolve microdomain-specific dynamics. Because both geNOps and GCaMP8s are genetically targetable, future versions of the dual construct could be directed to defined subcellular locales—such as the nuclear envelope, ER surface, postsynaptic densities, or perisynaptic regions—where nNOS is proposed to reside or be recruited [70]. Such spatially restricted sensors would enable us to distinguish global from microdomain Ca^{2+}–NO signaling, to determine whether nNOS is preferentially activated near particular channel types or synaptic sites, and to dissect how local NO production shapes downstream targets with distinct kinetics. In this sense, our current approach defines the temporal "logic" and threshold behavior of Ca^{2+}–nNOS coupling at the whole-cell level, while subcellularly targeted variants of the same dual biosensor will be essential to answer the remaining question of where in the neuron these critical NO signals are generated and sensed. However, the apparent "Ca^{2+} threshold" for NO production could not be quantified reliably in our dataset because the jGCaMP8s reporter behaves ultra sensitively under KCl depolarization, yielding near-saturating and highly similar Ca^{2+} transients at 10, 30, and 50 mM KCl. Consequently, dose–response or Ca^{2+}–NO correlation analyses (e.g., based on amplitude or AUC) are dominated by sensor saturation/compressed dynamic range rather than reflecting a true biological Ca^{2+} requirement for NO generation.

To provide a more intact physiological context, future studies will be required to implement dual-biosensor imaging in vivo or at least in acute brain slices; which is beyond the scope of the present study, which focuses on establishing and mechanistically characterizing Ca^{2+}–NO coupling in a controlled primary neuronal model under defined physioxic conditions.

4. Conclusion

In conclusion, we developed a bicistronic AAV-based dual biosensor that enables simultaneous, near-physiological imaging of Ca^{2+} and NO

in primary hippocampal neurons. Using this tool, we show that only strong depolarization crosses the Ca^{2+} threshold required for robust nNOS activation, whereas spontaneous and moderate Ca^{2+} activity remain largely NO-silent. Once produced, both endogenous and exogenous NO transiently suppress spontaneous Ca^{2+} spiking, revealing a bidirectional, thresholded coupling between these two signaling pathways. Our findings highlight the importance of physiological oxygen and temperature for faithfully capturing neuronal NO dynamics and provide a versatile platform that can be further adapted for subcellularly resolved Ca^{2+}–NO imaging in future studies.

5. Material methods

5.1. Buffer and solutions

All chemicals were obtained from NeoFroxx (Einhausen, Germany) unless otherwise stated. Imaging was performed in a HEPES-buffered saline solution containing 2 mM $CaCl_2$, 5 mM KCl, 138 mM NaCl, 1 mM $MgCl_2$, 10 mM HEPES, and 10 mM D-glucose (600-035 LG, Wisent Multicel) (pH adjusted to 7.42 with 1 M NaOH). Glutamate (Cat. No: 49 449-100G, Sigma Life Science) stock solution (100 mM) was freshly diluted to a final concentration of 30 μM for each experiment. For ATP stimulation experiments, ATP (34 369-07-8 Merck) stock solutions were freshly prepared on the day of imaging directly in HEPES-buffered saline and diluted to final concentrations of 5 μM and 30 μM. NOC-7 (Cat. No: ALX-430-018, Enzo) was stock solutions were prepared in deionized water and Proli NONOate (sc-222 190, Santa Cruz) was prepared in 50 mM NaOH.

5.2. Molecular cloning and AAV virus production

The bicistronic expression cassette encoding O-geNOp and jGCaMP8s separated by a P2A sequence (O-geNOp-P2A-jGCaMP8s) was synthesized de novo by Twist Bioscience and supplied as a sequence-verified DNA fragment (See supplementary note 1). On receipt, the insert was cloned into a pAAV2 backbone via the *Bam*HI and *Hin*dIII restriction sites. Ligation products were transformed into C3040 chemically competent *E. coli*, and individual colonies were screened by diagnostic restriction digestion to identify correctly assembled clones. The jGCaMP8s sensor sequence was originally obtained from Addgene (GCaMP8 series plasmid; gift deposit).

Recombinant AAV vectors were generated by triple transfection of HEK293T cells. Cells were maintained in DMEM supplemented with 10% fetal bovine serum and 1% penicillin–streptomycin at 37 °C in a humidified incubator with 5 kPa CO_2. For virus production, HEK293T cultures were grown to ~70% confluency and co-transfected with three plasmids: (i) the expression plasmid pAAV-hSyn-O-geNOp-P2A-jGCaMP8s, (ii) the adenoviral helper plasmid pHelper, and (iii) the rep/cap plasmid pRC encoding AAV2 replication functions and AAV9 capsid proteins. Plasmid DNA was delivered using polyethylenimine (PEI) in serum-reduced medium (Opti-MEM), at a DNA:PEI ratio of 1:4 (w/w), following standard PEI-mediated transfection procedures.

At 96 h post-transfection, cells and supernatants were collected. Cells were pelleted (300×*g*, 5 min), washed once with PBS (PBS-MK), and resuspended in lysis buffer containing 150 mM NaCl, 20 mM Tris-HCl, and 1 mM $MgCl_2$ (pH 8.0). Viral particles were released by three consecutive freeze–thaw cycles, followed by brief ultrasonic homogenization. Crude lysates were treated with Benzonase (Sigma, E8263) to degrade free nucleic acids and clarified by centrifugation (3000×*g*, 20 min, 4 °C) to remove cellular debris.

The clarified AAV-containing supernatant was purified by iodixanol density-gradient ultracentrifugation using OptiPrep™ Density Gradient Medium (iodixanol, Sigma, D1556). Lysates were layered onto a step gradient (17%, 25%, 40%, and 60% iodixanol) and centrifuged at ~220 000×*g* for 2 h at 4 °C. Virus-rich fractions were collected from the 40–60% interface, diluted in PBS supplemented with 5% D-sorbitol and 200 mM NaCl, and concentrated as well as buffer-exchanged using 100-kDa MWCO centrifugal filter units (Amicon® Ultra-15, 100K; Merck Millipore, cat. no. UFC910024). Final AAV preparations were aliquoted and stored at −80 °C until use.

Genomic titers of AAV stocks were determined by quantitative PCR targeting the WPRE element using specific primers (forward: 5′-GGCTGTGGGCATGACACT-3′; reverse: 5′-CCGAAGGAGCTGACGAA-3′). Titers are reported as genome copies per milliliter (GC/mL).

5.3. Primary and secondary cell culture

Primary neuron culture*:* Primary hippocampal, cerebellum and cortex neurons were extracted from mice aged postnatal day 0 to 3 (P0–P3). The neonatal mice were euthanized through decapitation, adhering to the ethical standards set by the institution. Brains were swiftly excised in a laminar flow hood and placed in an ice-cold dissection medium, specifically Hibernate-A (Gibco, Thermo Fisher Scientific; cat. A1247501) supplemented with 1% penicillin–streptomycin (100 × ; CAPRICORN SCI PS-B) and 1% stable L-glutamine (Stable Glutamine, 200 mM; Capricorn Scientific, cat. no. STA-B). Under a stereomicroscope, the hippocampi, cerebellum and cortex were carefully dissected and subsequently transferred into an enzyme digestion medium consisting of Leibovitz's L-15 (Gibco, Thermo Fisher Scientific; cat. 11415064) combined with 1% penicillin–streptomycin, 1% GlutaMAX, 1% NCS21 supplement (CAPRICORN SCI N2–K), 1% papain (Sigma, P4762) and 1% DNase I (Sigma, D5025). The tissue was incubated at 4 °C for 45 min.

Following enzymatic digestion, the hippocampi underwent gentle trituration using flame-polished Pasteur pipettes with progressively smaller diameters to generate a single-cell suspension. This homogenate was then transferred into an enzyme inhibition medium composed of L-15 supplemented with 1% penicillin–streptomycin, 1% GlutaMAX, 1% NCS21, and 10% fetal bovine serum (FBS; Gibco, Thermo Fisher Scientific; cat. 10270106) and incubated for an additional 15 min at 4 °C. Cells were pelleted via centrifugation at 1000 rpm for 5 min, resuspended in a permanent culture medium (Neurobasal-A; Gibco, Thermo Fisher Scientific; cat. 10888022) supplemented with 1% penicillin–streptomycin, 1% GlutaMAX, 1% NCS21, and 1% horse serum (CAPRICORN; HOS-1A), and plated for subsequent experiments.

After plating, cultures were placed either in a physioxic incubator (5 kPa O_2, 5 kPa CO_2, balance N_2) or maintained in a standard incubator approximating atmospheric oxygen (18 kPa O_2, 5 kPa CO_2). Neurons remained in these respective oxygen conditions until the experimental endpoint. On the evening of the plating day, culture wells were topped up to the final volume with pre-equilibrated Neurobasal-A medium, and on the following day in vitro (DIV1) neurons were transduced with the respective AAV constructs at a final dose of 3×10^9 viral genomes (vg) per well.

Primary dorsal root ganglion (DRG) neuron culture: Primary DRG neurons were isolated from 6–8-week-old male mice. Animals were anesthetized by intraperitoneal injection of ketamine (100 mg/kg) and xylazine (10 mg/kg) and sacrificed by cervical dislocation. Cervical, thoracic, and lumbar dorsal root ganglia were dissected and transferred into RPMI-1640 (Gibco, Thermo Fisher Scientific; cat. 21875034) containing 1% penicillin–streptomycin. DRGs were subjected to sequential enzymatic digestion at 37 °C: first with collagenase (100 U/mL, 50 min; Sigma, C7657), followed by trypsin (1 mg/mL, 15 min; Sigma, T4549), and finally DNase I (50 μg/mL, 30 min; Sigma, D5025). Between and after digestion steps, the tissue was gently triturated by serial pipetting, and the resulting suspension was passed three times through a 26-gauge needle to further dissociate remaining aggregates.

Enzymes were removed by centrifugation at 120×*g* for 3 min, and the cell pellet was resuspended in primary neuron culture medium supplemented with 10% FBS (Gibco, Thermo Fisher Scientific; cat. 10270106). DRG neurons were enriched using a discontinuous Percoll density gradient (60%, 35%, 10%) and collected from the 35% interface.

The enriched fraction was washed once with Neurobasal-A (Gibco, Thermo Fisher Scientific; cat. 10888022), centrifuged again at 120×*g* for 3 min, resuspended in primary neuron culture medium, and plated onto poly-L-lysine/laminin-coated glass-bottom dishes. DRG neuron cultures were maintained at 37 °C and 5 kPa CO_2.

Secondary cell culture (HEK293T) and transfection: Human embryonic kidney cells (HEK293T) were maintained in high-glucose Dulbecco's modified Eagle medium (DMEM, 4.5 g/L glucose, with pyruvate; Gibco, Thermo Fisher Scientific; cat. 41966029) supplemented with 10% FBS (Gibco, Thermo Fisher Scientific; cat. 10270106), 100 U/mL penicillin, and 100 μg/mL streptomycin (100 × ; CAPRICORN SCI PS-B) in a humidified incubator at 37 °C and 5 kPa CO_2. For imaging experiments, cells were seeded one day prior to transfection onto 30 mm glass coverslips (No. 1; Glaswarenfabrik Karl Knecht, Sondheim, Germany) placed in 6-well plates.

All experiments with primary neurons were performed between the 4^{th} and 6^{th} week after neuronal isolation. Independent repeats were carried out in separate culture dishes derived from the same animal. Figs. 1–3 datasets each originate from different animals, while Fig. 4 combines experiments performed using three additional animals independent from previous figures.

HEK293T cells were transfected with the bicistronic construct hSyn-O-geNOp-P2A-GCaMP8s using polyethylenimine (PEI) at a DNA:PEI ratio of 1:5 in Opti-MEM I reduced-serum medium with GlutaMAX supplement (Gibco, Thermo Fisher Scientific; cat. 51985034), according to the manufacturer's recommendations. Approximately 24 h after transfection, cells on coverslips were transferred to the imaging chamber and used for live-cell fluorescence experiments.

5.4. Immunolabeling

Adult DRG, and neonatal cerebellar, cortical and hippocampal neuronal cultures were immunolabeled for nNOS and pan neural marker TUJ-1. First, the cells were fixed in 4% paraformaldehyde (PFA) for 15 min at RT. Then, the cells were treated in a blocking buffer containing 3% bovine serum albumin (BSA), 0.01% sodium azide, 5% serum, and 0.1% Triton X-100 in PBS for 1 h. After incubation, the cells were washed with PBS and incubated with primary antibodies, rabbit anti-nNOS (1:200; 4231, Santa Cruz) and TUJ-1 conjugated with Alexa Fluor 488 (1:500; 169 556, Abcam) in a dilution buffer (3% bovine serum albumin (BSA), 0.01% sodium azide, 5% serum, and 1% Tween-20 in PBS) at 4 °C for overnight. The following day, the cells were treated with and Alexa Fluor 647 anti-rabbit IgG (1:500; ab150083, Abcam) secondary antibody for 1 h at RT. For nuclear staining, the cells were stained with DAPI (1 μg/ml; D9542, Sigma) for 5 min at RT. After 2-3 times PBS washing, fresh PBS was added into each well prior to confocal imaging.

5.5. Epifluorescence and confocal imaging

Live-cell widefield epifluorescence imaging was performed using a Zeiss Axio Observer Z1.7 inverted microscope (Carl Zeiss AG, Oberkochen, Germany) equipped with Plan-Apochromat 20 × /0.8 dry objective and an Axiocam 503 monochrome CCD camera. Neurons were imaged in an NGFI perfusion chamber connected to a custom pump-driven perfusion system that enabled rapid delivery and washout of pharmacological agents and imaging buffer. For O-geNOp imaging, cells were excited with a 555/30 nm LED light source (Colibri 7), and fluorescence emission was collected using an FT570 dichroic beamsplitter and a 605/70 nm emission filter; the same optical setup was used for both single- and dual-biosensor recordings. EGFP or GCaMP fluorescence was recorded using 470/40 nm LED excitation and a 525/50 nm emission filter with the corresponding dichroic element, and alternating acquisition modes were used during dual imaging to avoid spectral overlap. Prior to imaging, cells were pre-treated for 15 min with $FeSO_4$ and ascorbate (concentrations detailed in the Results section) to achieve full activation of the geNOps biosensor, as described previously [36]. All buffers and culture media were pre-equilibrated at 5 kPa O_2 for at least 2 h, and in most cases overnight, prior to use. Right prior to any imaging experiment, the pH of all imaging media was double checked after oxygen adaptation. Media exchanges were performed rapidly (within a few seconds) to minimize exposure to ambient air and prevent detectable alterations in pH or oxygen levels during the 15-min iron incubation period. Experimental procedures requiring prolonged handling were carried out in a custom oxygen-regulated glove box, ensuring stable and defined O_2 conditions throughout the manipulation.

The nNOS and TUJ-1 immunolabeled DRG, cerebellar, cortical and hippocampal cells were imaged under LSM 780 scanning confocal microscopy (Carl Zeiss) equipped with Plan-Apochromat 20x/0.8 M27 objective. 488 nm and 633 nm laser light for excitation and 493-628 nm and 638-747 nm emission filters were used to detect Alexa Fluor 488 nm and Alexa Fluor 633, respectively. 2856 x 2856 image size pixels, 1x1 binning mode and 4 for averaging were selected to obtain high resolution images. Detector gain and digital gain was set to 800 and 1, respectively.

5.6. Statistical analysis

All imaging data were analyzed using GraphPad Prism Software version 9 (GraphPad Software, San Diego, CA, USA). All experiments were performed at least three times and indicated as n where n represents the number of different experimental cultures. For dual-color simultaneous NO–Ca^{2+} imaging, each trace show representative examples from repeated experiments (at least three, as indicated in the figure legend).

All data denote mean ± S.D. unless stated otherwise. Statistical analysis of multiple groups was performed using one-way ANOVA with Tukey's posttest (Comparison of all pairs of columns). P-values are indicated as numerical values. For the comparison of multiple groups, the P-value was not indicated if the P-value was higher than 0.05. In order to compare two experimental conditions, an unpaired Student's t-test was performed. Statistical analysis of two groups was performed using unpaired Student's t-test.

Multiple neurons or ROIs recorded within a single dish were treated as technical replicates. For image analysis, ROIs were manually defined around individual neuronal somata using fluorescence intensity and morphology as selection criteria. Only well-isolated, morphologically intact neurons were included. Typically, 1-2 neuronal ROIs were analyzed per field of view, depending on cell density. Fluorescence traces were extracted for each ROI individually and analyzed on a per-neuron basis.

5.7. Calcium spike detection and frequency analysis

For each neuron, jGCaMP fluorescence signals were analyzed independently using neuron-specific time intervals. Raw fluorescence traces were used directly for spike detection. Calcium spikes were detected in MATLAB (R2025a) using the *findpeaks* function applied to the raw signal, enforcing (i) a minimum inter-spike interval using a *MinPeakDistance* of 0.2 min (12 s, corresponding to approximately four imaging frames at the acquisition rate) to prevent multiple detections of closely spaced local maxima, and (ii) a minimum peak prominence threshold using a *MinPeakProminence* of 3 a. u. to exclude small fluctuations that do not represent clear spike events. Spike frequency was calculated for each neuron as the number of detected peaks divided by the recording duration (spikes/min), where duration was defined as the difference between the first and last valid time points for that neuron. Baseline and during-NO periods were quantified separately for each neuron.

Ethics

All animal experiments were approved by the Institutional Animal

Care and Use Committee of Istanbul Medipol University (ethics approval no. E−38828770-604.01-7880 and E−38828770-772.02-6554) and conducted in accordance with national and institutional guidelines.

Declaration of generative AI and AI-assisted technologies in the manuscript preparation process

During the preparation of this work the authors used ChatGPT as a support tool for language editing and MATLAB code drafting. After using this tool, the authors reviewed and edited the content as needed and take full responsibility for the content of the published article.

Funding resources

This work was supported by the EMBO Installation Grant (EMBO IG J4113) awarded to E.E.; the ERA-NET NEURON JTC2022 program to P. G., N·P, and E.E. that was co-funded through the Scientific and Technological Research Council of Türkiye (TÜBİTAK, Grant No. 123N411) awarded to E.E.; and the TÜBİTAK 2218 Fellowship (Grant No. 121C392) awarded to T.A.C. and E.E. P.G. was supported by Inserm, Université Paris Cité, and Fondation Princesse Grace de Monaco.

CRediT authorship contribution statement

Asel Aydeger: Conceptualization, Formal analysis, Methodology, Validation, Visualization, Writing – original draft, Writing – review & editing. **Sena Yildirim:** Conceptualization, Formal analysis, Methodology, Validation, Visualization, Writing – original draft, Writing – review & editing. **Tuba Akgul Caglar:** Conceptualization, Data curation, Formal analysis, Methodology, Validation, Visualization, Writing – original draft, Writing – review & editing. **Asal Ghaffari Zaki:** Conceptualization, Data curation, Formal analysis, Methodology, Validation, Visualization, Writing – original draft, Writing – review & editing. **Seyed Mohammad Miri:** Conceptualization, Data curation, Formal analysis, Methodology, Validation, Visualization, Writing – original draft, Writing – review & editing. **Joudi Armouch:** Data curation, Formal analysis, Methodology, Validation, Visualization, Writing – original draft, Writing – review & editing. **Hamzah Issa:** Conceptualization, Formal analysis, Methodology, Validation, Visualization, Writing – original draft, Writing – review & editing. **Esranur Yavuz:** Formal analysis, Methodology, Visualization. **Arda Kebapçı:** Project administration, Validation. **Mehmet Koçak:** Data curation, Methodology. **Roland Malli:** Conceptualization, Supervision, Writing – original draft, Writing – review & editing. **Pierre Gressens:** Supervision, Writing – review & editing. **Nikolaus Plesnila:** Supervision, Writing – review & editing. **Emrah Eroglu:** Conceptualization, Formal analysis, Funding acquisition, Investigation, Methodology, Resources, Supervision, Validation, Visualization, Writing – original draft, Writing – review & editing.

Declaration of competing interest

The authors declare that they have no known competing financial interests or personal relationships that could have appeared to influence the work reported in this paper.

Acknowledgment

We thank the following researchers and Addgene for providing plasmids: AAV-hSyn-Soma-jGCaMP8s, a gift from Marianne Fyhn (Addgene plasmid #169256; http://n2t.net/addgene:169256; RRID: Addgene_169256); AAV-CAG-jGCaMP8f-WPRE, a gift from Loren Looger (Addgene plasmid #179254; http://n2t.net/addgene:179254; RRID: Addgene_179254); and pAAV.Syn.GCaMP6s.WPRE.SV40, a gift from Douglas Kim & the GENIE Project (Addgene plasmid #100843; http://n2t.net/addgene:100843; RRID:Addgene_100843).

Appendix A. Supplementary data

Supplementary data to this article can be found online at https://doi.org/10.1016/j.redox.2026.104094.

Data availability

Data will be made available on request.

References

[1] J. Garthwaite, From synaptically localized to volume transmission by nitric oxide, J. Physiol. 594 (1) (2016) 9–18, https://doi.org/10.1113/JP270297.
[2] S.A. Bradley, J.R. Steinert, Nitric oxide-mediated posttranslational modifications: impacts at the synapse, Oxid. Med. Cell. Longev. 2016 (2016) 5681036, https://doi.org/10.1155/2016/5681036.
[3] U. Förstermann, W.C. Sessa, Nitric oxide synthases: regulation and function, Eur. Heart J. 33 (7) (2012) 829–837, https://doi.org/10.1093/eurheartj/ehr304, 837a–837d.
[4] K.S. Korshunov, M. Prakriya, Store-Operated calcium channels in the nervous System, Annu. Rev. Physiol. 87 (1) (2025) 173–199, https://doi.org/10.1146/annurev-physiol-022724-105330.
[5] D.D. Thomas, L.A. Ridnour, J.S. Isenberg, W. Flores-Santana, C.H. Switzer, S. Donzelli, P. Hussain, C. Vecoli, N. Paolocci, S. Ambs, C.A. Colton, C.C. Harris, D. D. Roberts, D.A. Wink, The chemical biology of nitric oxide: implications in cellular signaling, Free Radic. Biol. Med. 45 (1) (2008) 18–31, https://doi.org/10.1016/j.freeradbiomed.2008.03.020.
[6] J.S. Stamler, S. Lamas, F.C. Fang, Nitrosylation. the prototypic redox-based signaling mechanism, Cell 106 (6) (2001) 675–683, https://doi.org/10.1016/s0092-8674(01)00495-0.
[7] G.C. Brown, V. Borutaite, Nitric oxide inhibition of mitochondrial respiration and its role in cell death, Free Radic. Biol. Med. 33 (11) (2002) 1440–1450, https://doi.org/10.1016/s0891-5849(02)01112-7.
[8] N. Toda, K. Ayajiki, T. Okamura, Cerebral blood flow regulation by nitric oxide: recent advances, Pharmacol. Rev. 61 (1) (2009) 62–97, https://doi.org/10.1124/pr.108.000547.
[9] V. Calabrese, C. Mancuso, M. Calvani, E. Rizzarelli, D.A. Butterfield, A.M.G. Stella, Nitric oxide in the central nervous System: neuroprotection versus neurotoxicity, Nat. Rev. Neurosci. 8 (10) (2007) 766–775, https://doi.org/10.1038/nrn2214.
[10] R.A. Dulce, V. Mayo, E.B. Rangel, W. Balkan, J.M. Hare, Interaction between neuronal nitric oxide synthase signaling and temperature influences sarcoplasmic reticulum calcium leak: role of nitroso-redox balance, Circ. Res. 116 (1) (2015) 46–55, https://doi.org/10.1161/CIRCRESAHA.116.305172.
[11] J.R. Hickok, D. Vasudevan, K. Jablonski, D.D. Thomas, Oxygen dependence of nitric oxide-mediated signaling, Redox Biol. 1 (1) (2013) 203–209, https://doi.org/10.1016/j.redox.2012.11.002.
[12] K. Chachlaki, V. Prevot, Nitric oxide signalling in the brain and its control of bodily functions, Br. J. Pharmacol. 177 (24) (2020) 5437–5458, https://doi.org/10.1111/bph.14800.
[13] Y. Hayashi, M. Nishio, Y. Naito, H. Yokokura, Y. Nimura, H. Hidaka, Y. Watanabe, Regulation of neuronal nitric-oxide synthase by Calmodulin Kinases, J. Biol. Chem. 274 (29) (1999) 20597–20602, https://doi.org/10.1074/jbc.274.29.20597.
[14] G. Zündorf, G. Reiser, Calcium dysregulation and homeostasis of neural calcium in the molecular mechanisms of neurodegenerative diseases provide multiple targets for neuroprotection, Antioxidants Redox Signal. 14 (7) (2011) 1275–1288, https://doi.org/10.1089/ars.2010.3359.
[15] S. Kakizawa, T. Yamazawa, Y. Chen, A. Ito, T. Murayama, H. Oyamada, N. Kurebayashi, O. Sato, M. Watanabe, N. Mori, K. Oguchi, T. Sakurai, H. Takeshima, N. Saito, M. Iino, Nitric oxide-induced calcium release via ryanodine receptors regulates neuronal function, EMBO J. 31 (2) (2012) 417–428, https://doi.org/10.1038/emboj.2011.386.
[16] G.P. Ahern, V.A. Klyachko, M.B. Jackson, cGMP and S-Nitrosylation: two routes for modulation of neuronal excitability by NO, Trends Neurosci. 25 (10) (2002) 510–517, https://doi.org/10.1016/s0166-2236(02)02254-3.
[17] A.J.B. Tozer, I.D. Forsythe, J.R. Steinert, Nitric oxide signalling augments neuronal voltage-gated L-Type (Ca(v)1) and P/q-Type (Ca(v)2.1) channels in the mouse medial nucleus of the trapezoid body, PLoS One 7 (2) (2012) e32256, https://doi.org/10.1371/journal.pone.0032256.
[18] Z.H. Kalati, O. Gholami, B. Amin, A. Pejhan, S. Sahab-Negah, M. Gholami, H. Azhdari-Zarmehri, M. Mohammad-Zadeh, The role of 5-HT1A receptors and neuronal nitric oxide synthase in a seizur induced kindling model in rats, Neurochem. Res. 47 (7) (2022) 1934–1942, https://doi.org/10.1007/s11064-022-03577-1.
[19] K.L.H. Wu, Y.-M. Chao, S.-J. Tsay, C.H. Chen, S.H.H. Chan, I. Dovinova, J.Y. H. Chan, Role of nitric oxide synthase uncoupling at rostral ventrolateral medulla in redox-sensitive hypertension associated with Metabolic syndrome, Hypertension 64 (4) (2014) 815–824, https://doi.org/10.1161/HYPERTENSIONAHA.114.03777.
[20] J.G. Spiers, J.R. Steinert, Nitrergic modulation of ion channel function in regulating neuronal excitability, Channels 15 (1) (2021) 666–679, https://doi.org/10.1080/19336950.2021.2002594.
[21] R.A. Sokolov, D. Jappy, O.V. Podgorny, I.V. Mukhina, Nitric oxide synthase blockade impairs spontaneous calcium activity in Mouse primary hippocampal

culture cells, Int. J. Mol. Sci. 24 (3) (2023) 2608, https://doi.org/10.3390/ijms24032608.
[22] Y. Wang, F. Hong, S. Yang, Roles of nitric oxide in brain ischemia and reperfusion, Int. J. Mol. Sci. 23 (8) (2022) 4243, https://doi.org/10.3390/ijms23084243.
[23] L. Cherian, R. Hlatky, C.S. Robertson, Nitric oxide in traumatic brain injury, Brain Pathol. 14 (2) (2004) 195–201, https://doi.org/10.1111/j.1750-3639.2004.tb00053.x.
[24] L. Wang, D. Lu, X. Wang, Z. Wang, W. Li, G. Chen, The effects of nitric oxide in alzheimer's disease, Med. Gas Res. 14 (4) (2024) 186–191, https://doi.org/10.4103/2045-9912.385939.
[25] L. Zhang, V.L. Dawson, T.M. Dawson, Role of nitric oxide in parkinson's disease, Pharmacol. Ther. 109 (1–2) (2006) 33–41, https://doi.org/10.1016/j.pharmthera.2005.05.007.
[26] N. Üremiş, M.M. Üremiş, Oxidative/Nitrosative stress, apoptosis, and Redox signaling: key players in neurodegenerative diseases, J. Biochem. Mol. Toxicol. 39 (1) (2025) e70133, https://doi.org/10.1002/jbt.70133.
[27] V.C. Stewart, S.J.R. Heales, Nitric oxide-induced mitochondrial dysfunction: implications for neurodegeneration, Free Radic. Biol. Med. 34 (3) (2003) 287–303, https://doi.org/10.1016/s0891-5849(02)01327-8.
[28] R. Radi, Nitric oxide, oxidants, and protein tyrosine nitration, Proc. Natl. Acad. Sci. U. S. A. 101 (12) (2004) 4003–4008, https://doi.org/10.1073/pnas.0307446101.
[29] A. Mannan, T.G. Singh, Mechanistic correlation of potassium channel sensing and nitric oxide activity in neuroinflammation, Mol. Biol. Rep. 52 (1) (2025) 874, https://doi.org/10.1007/s11033-025-10954-w.
[30] R. Balez, C.H. Stevens, K. Lenk, S. Maksour, K. Sidhu, G. Sutherland, L. Ooi, Increased neuronal nitric oxide synthase in alzheimer's disease mediates spontaneous calcium signaling and divergent glutamatergic calcium responses, Antioxidants Redox Signal. 41 (4–6) (2024) 255–277, https://doi.org/10.1089/ars.2023.0395.
[31] N. Toda, K. Ayajiki, T. Okamura, Cerebral blood flow regulation by nitric oxide in neurological disorders, Can. J. Physiol. Pharmacol. 87 (8) (2009) 581–594, https://doi.org/10.1139/y09-048.
[32] N. Hardingham, J. Dachtler, K. Fox, The role of nitric oxide in pre-synaptic plasticity and homeostasis, Front. Cell. Neurosci. 7 (2013) 190, https://doi.org/10.3389/fncel.2013.00190.
[33] H.Y. Altun, M. Secilmis, F. Yang, T. Akgul Caglar, E. Vatandaslar, M.F. Toy, S. Vilain, G.E. Mann, G. Öztürk, E. Eroglu, Visualizing hydrogen peroxide and nitric oxide dynamics in endothelial cells using multispectral imaging under controlled oxygen conditions, Free Radic. Biol. Med. 221 (2024) 89–97, https://doi.org/10.1016/j.freeradbiomed.2024.05.021.
[34] S.M. Miri, B.N. Ata, Ş. Çimen, S. Barakat, A. Ghaffari Zaki, J. Armouch, E. Vatandaşlar, S. Vilain, G. Öztürk, E. Eroğlu, Development of an oxygen-insensitive Nrf2 reporter reveals redox regulation under physiological Normoxia, ACS Sens. (2025), https://doi.org/10.1021/acssensors.4c03167.
[35] S. Barakat, F. Yang, H.E. Yelkenci, K. Kök, G.E. Mann, E. Eroğlu, Proteomic data and drug implications for cerebral microvascular endothelial cells under varying oxygen levels, Sci. Data 12 (1) (2025) 989, https://doi.org/10.1038/s41597-025-05160-z.
[36] G. Sevimli, M.J. Smith, T.A. Caglar, Ş. Bilir, M. Secilmis, H.Y. Altun, E.N. Yigit, F. Yang, T.P. Keeley, R. Malli, G. Öztürk, G.E. Mann, E. Eroglu, Nitric oxide biosensor uncovers diminished ferrous iron-dependency of cultured cells adapted to physiological oxygen levels, Redox Biol. 53 (2022) 102319, https://doi.org/10.1016/j.redox.2022.102319.
[37] T.P. Keeley, G.E. Mann, Defining physiological normoxia for improved translation of cell physiology to animal models and humans, Physiol. Rev. 99 (1) (2019) 161–234, https://doi.org/10.1152/physrev.00041.2017.
[38] T.P. Keeley, R.C.M. Siow, R. Jacob, G.E. Mann, A PP2A-Mediated feedback mechanism controls Ca2+ -Dependent NO synthesis under physiological oxygen, FASEB J. 31 (12) (2017) 5172–5183, https://doi.org/10.1096/fj.201700211R.
[39] E. Eroglu, S. Hallström, H. Bischof, M. Opelt, K. Schmidt, B. Mayer, M. Waldeck-Weiermair, W.F. Graier, R. Malli, Real-Time visualization of distinct nitric oxide generation of nitric oxide synthase isoforms in single cells, Nitric Oxide 70 (2017) 59–67, https://doi.org/10.1016/j.niox.2017.09.001.
[40] R.A. Hunter, W.L. Storm, P.N. Coneski, M.H. Schoenfisch, Inaccuracies of nitric oxide measurement methods in biological media, Anal. Chem. 85 (3) (2013) 1957–1963, https://doi.org/10.1021/ac303787p.
[41] L.E. McQuade, S.J. Lippard, Fluorescent probes to investigate nitric oxide and other reactive nitrogen species in biology (truncated form: fluorescent probes of reactive nitrogen species), Curr. Opin. Chem. Biol. 14 (1) (2010) 43–49, https://doi.org/10.1016/j.cbpa.2009.10.004.
[42] Y. Zhang, M. Rózsa, Y. Liang, D. Bushey, Z. Wei, J. Zheng, D. Reep, G.J. Broussard, A. Tsang, G. Tsegaye, S. Narayan, C.J. Obara, J.-X. Lim, R. Patel, R. Zhang, M. B. Ahrens, G.C. Turner, S.S.-H. Wang, W.L. Korff, E.R. Schreiter, K. Svoboda, J. P. Hasseman, I. Kolb, L.L. Looger, Fast and sensitive GCaMP calcium indicators for imaging neural populations, Nature 615 (7954) (2023) 884–891, https://doi.org/10.1038/s41586-023-05828-9.
[43] E. Eroglu, B. Gottschalk, S. Charoensin, S. Blass, H. Bischof, R. Rost, C.T. Madreiter-Sokolowski, B. Pelzmann, E. Bernhart, W. Sattler, S. Hallström, T. Malinski, M. Waldeck-Weiermair, W.F. Graier, R. Malli, Development of novel FP-Based probes for live-cell imaging of nitric oxide dynamics, Nat. Commun. 7 (1) (2016) 10623, https://doi.org/10.1038/ncomms10623.
[44] E. Eroglu, S.S.S. Saravi, A. Sorrentino, B. Steinhorn, T. Michel, Discordance between eNOS phosphorylation and activation revealed by multispectral imaging and chemogenetic methods, Proc. Natl. Acad. Sci. U. S. A. 116 (40) (2019) 20210–20217, https://doi.org/10.1073/pnas.1910942116.
[45] E. Eroglu, S. Charoensin, H. Bischof, J. Ramadani, B. Gottschalk, M.R. Depaoli, M. Waldeck-Weiermair, W.F. Graier, R. Malli, Genetic biosensors for imaging nitric oxide in single cells, Free Radic. Biol. Med. 128 (2018) 50–58, https://doi.org/10.1016/j.freeradbiomed.2018.01.027.
[46] A. Ledo, R.M. Barbosa, J. Frade, J. Laranjinha, Nitric oxide monitoring in hippocampal brain slices using electrochemical methods, Methods Enzymol. 359 (2002) 111–125, https://doi.org/10.1016/s0076-6879(02)59176-x.
[47] T.F.W. Horn, G. Wolf, S. Duffy, S. Weiss, G. Keilhoff, B.A. MacVicar, Nitric oxide promotes intracellular calcium release from Mitochondria in striatal neurons, FASEB J. 16 (12) (2002) 1611–1622, https://doi.org/10.1096/fj.02-0126com.
[48] L.R. Zhong, S. Estes, L. Artinian, V. Rehder, Nitric oxide regulates neuronal activity via calcium-activated potassium channels, PLoS One 8 (11) (2013) e78727, https://doi.org/10.1371/journal.pone.0078727.
[49] S. Blackshaw, M.J.L. Eliasson, A. Sawa, C.C. Watkins, D. Krug, A. Gupta, T. Arai, R. J. Ferrante, S.H. Snyder, Species, strain and developmental variations in hippocampal neuronal and endothelial nitric oxide synthase clarify discrepancies in nitric oxide-dependent synaptic plasticity, Neuroscience 119 (4) (2003) 979–990, https://doi.org/10.1016/s0306-4522(03)00217-3.
[50] C.L.M. Bon, J. Garthwaite, On the role of nitric oxide in hippocampal long-term potentiation, J. Neurosci. 23 (5) (2003) 1941–1948, https://doi.org/10.1523/JNEUROSCI.23-05-01941.2003.
[51] P.A. Reis, C. F. G. de Albuquerque, T. Maron-Gutierrez, A.R. Silva, H.C. Neto, C. F. de, P.A. Reis, C. F. G. de Albuquerque, T. Maron-Gutierrez, A.R. Silva, H.C. Neto, C.F. de, Role of nitric oxide synthase in the function of the central nervous System under normal and infectious conditions, in: Nitric Oxide Synthase - Simple Enzyme-Complex Roles, IntechOpen, 2017, https://doi.org/10.5772/67816.
[52] M. Kavdia, A.S. Popel, Contribution of nNOS- and eNOS-Derived NO to Microvascular smooth muscle NO exposure, J. Appl. Physiol. 97 (1) (2004) 293–301, https://doi.org/10.1152/japplphysiol.00049.2004, 1985.
[53] C.F. Lourenço, J. Laranjinha, Nitric oxide pathways in neurovascular coupling under normal and stress conditions in the brain: strategies to rescue aberrant coupling and improve cerebral blood flow, Front. Physiol. 12 (2021) 729201, https://doi.org/10.3389/fphys.2021.729201.
[54] R.L. Hoiland, H.G. Caldwell, C.A. Howe, D. Nowak-Flück, B.S. Stacey, D.M. Bailey, J.F.R. Paton, D.J. Green, M.S. Sekhon, D.B. Macleod, P.N. Ainslie, Nitric oxide is fundamental to neurovascular coupling in humans, J. Physiol. 598 (21) (2020) 4927–4939, https://doi.org/10.1113/JP280162.
[55] J.S. Gonçalves, R.M. Seiça, J. Laranjinha, C.F. Lourenço, Impairment of Neurovascular coupling in the hippocampus due to decreased nitric oxide bioavailability supports early cognitive dysfunction in type 2 diabetic rats, Free Radic. Biol. Med. 193 (Pt 2) (2022) 669–675, https://doi.org/10.1016/j.freeradbiomed.2022.11.009.
[56] L. Tricoire, T. Vitalis, Neuronal nitric oxide synthase expressing neurons: a journey from birth to neuronal circuits, Front. Neural Circ. 6 (2012) 82, https://doi.org/10.3389/fncir.2012.00082.
[57] E. Levin, H. Diekmann, D. Fischer, Highly efficient transduction of primary adult CNS and PNS neurons, Sci. Rep. 6 (2016) 38928, https://doi.org/10.1038/srep38928.
[58] Z. Liu, O. Chen, J.B.J. Wall, M. Zheng, Y. Zhou, L. Wang, H.R. Vaseghi, L. Qian, J. Liu, Systematic comparison of 2A peptides for cloning multi-genes in a polycistronic vector, Sci. Rep. 7 (1) (2017) 2193, https://doi.org/10.1038/s41598-017-02460-2.
[59] T.P. Keeley, R.C.M. Siow, R. Jacob, G.E. Mann, A PP2A-Mediated feedback mechanism controls Ca2+ -Dependent NO synthesis under physiological oxygen, FASEB J. 31 (12) (2017) 5172–5183, https://doi.org/10.1096/fj.201700211R.
[60] P.-R. Wu, C.-C. Kuo, S.-F. Yet, J.-Y. Liou, K.K. Wu, P.-F. Chen, Lobe-Specific calcium binding in Calmodulin regulates Endothelial nitric oxide synthase activation, PLoS One 7 (6) (2012) e39851, https://doi.org/10.1371/journal.pone.0039851.
[61] J. Tejero, M.M. Haque, D. Durra, D.J. Stuehr, A bridging interaction allows Calmodulin to activate NO synthase through a Bi-Modal mechanism, J. Biol. Chem. 285 (34) (2010) 25941–25949, https://doi.org/10.1074/jbc.M110.126797.
[62] T.I.A. Evans, M.A. Shea, Energetics of Calmodulin domain interactions with the Calmodulin binding domain of CaMKII, Proteins 76 (1) (2009) 47–61, https://doi.org/10.1002/prot.22317.
[63] H.Y. Park, S.A. Kim, J. Korlach, E. Rhoades, L.W. Kwok, W.R. Zipfel, M. N. Waxham, W.W. Webb, L. Pollack, Conformational changes of Calmodulin upon Ca2+ binding studied with a microfluidic mixer, Proc. Natl. Acad. Sci. U. S. A. 105 (2) (2008) 542–547, https://doi.org/10.1073/pnas.0710810105.
[64] D.E. Spratt, E. Newman, J. Mosher, D.K. Ghosh, J.C. Salerno, J.G. Guillemette, Binding and activation of nitric oxide synthase isozymes by Calmodulin EF hand pairs, FEBS J. 273 (8) (2006) 1759–1771, https://doi.org/10.1111/j.1742-4658.2006.05193.x.
[65] M.G. Campbell, B.C. Smith, C.S. Potter, B. Carragher, M.A. Marletta, Molecular Architecture of Mammalian nitric oxide synthases, Proc. Natl. Acad. Sci. U. S. A. 111 (35) (2014) E3614–E3623, https://doi.org/10.1073/pnas.1413763111.
[66] N. Heim, O. Garaschuk, M.W. Friedrich, M. Mank, R.I. Milos, Y. Kovalchuk, A. Konnerth, O. Griesbeck, Improved calcium imaging in transgenic mice expressing a Troponin C-Based biosensor, Nat. Methods 4 (2) (2007) 127–129, https://doi.org/10.1038/nmeth1009.
[67] S.R. Vincent, Nitric oxide neurons and neurotransmission, Prog. Neurobiol. 90 (2) (2010) 246–255, https://doi.org/10.1016/j.pneurobio.2009.10.007.
[68] L. Artinian, L. Zhong, H. Yang, V. Rehder, Nitric oxide as intracellular modulator: internal production of NO increases neuronal excitability via modulation of several

ionic conductances, Eur. J. Neurosci. 36 (10) (2012) 3333–3343, https://doi.org/10.1111/j.1460-9568.2012.08260.x.

[69] M. Canossa, E. Giordano, S. Cappello, C. Guarnieri, S. Ferri, Nitric oxide down-regulates brain-derived neurotrophic factor secretion in cultured hippocampal neurons, Proc. Natl. Acad. Sci. U. S. A. 99 (5) (2002) 3282–3287, https://doi.org/10.1073/pnas.042504299.

[70] M.A. Packer, Y. Stasiv, A. Benraiss, E. Chmielnicki, A. Grinberg, H. Westphal, S. A. Goldman, G. Enikolopov, Nitric oxide negatively regulates Mammalian adult neurogenesis, Proc. Natl. Acad. Sci. U. S. A. 100 (16) (2003) 9566–9571, https://doi.org/10.1073/pnas.1633579100.